

Laser fragmentation in liquid synthesis of novel palladium-sulfur compound nanoparticles as efficient electrocatalysts for hydrogen evolution reaction

Guo-Shuai Fu(付国帅)†, Hong-Zhi Gao(高宏志)†, Guo-Wei Yang(杨国伟), Peng Yu(于鹏)‡, and Pu Liu(刘璞)§

Citation: Chin. Phys. B, 2022, 31 (7): 077901 DOI: 10.1088/1674-1056/ /ac4e0e
Journal homepage: http://cpb.iphy.ac.cn; http://iopscience.iop.org/cpb

What follows is a list of articles you may be interested in

Prediction of structured void-containing 1T-$PtTe_2$ monolayer with potential catalytic activity for hydrogen evolution reaction

Bao Lei(雷宝), Yu-Yang Zhang(张余洋), Shi-Xuan Du(杜世萱)
Chin. Phys. B, 2020, 29 (**5**): 058104. DOI: 10.1088/1674-1056/ab8203

Time-resolved shadowgraphs and morphology analyses of aluminum ablation with multiple femtosecond laser pulses

Zehua Wu(吴泽华), Nan Zhang(张楠), Xiaonong Zhu(朱晓农), Liqun An(安力群), Gangzhi Wang(王刚志), Ming Tan(谭明)
Chin. Phys. B, 2018, 27 (**7**): 077901. DOI: 10.1088/1674-1056/27/7/077901

Self-organized voids revisited： Experimental verification of the formation mechanism

Song Juan, Ye Jun-Yi, Qian Meng-Di, Luo Fang-Fang, Lin Xian, Bian Hua-Dong, Dai Ye, Ma Guo-Hong, Chen Qing-Xi, Jiang Yan, Zhao Quan-Zhong, Qiu Jian-Rong
Chin. Phys. B, 2014, 23 (**7**): 077901. DOI: 10.1088/1674-1056/23/7/077901

Suppressing the mechanical quadrature error of a quartz double-H gyroscope through laser trimming

Zhao Ke, Feng Li-Hui, Wang Qian-Qian, Liu Ming-Zhi, Wang Ben-Guo, Cui Fang, Sun Yu-Nan
Chin. Phys. B, 2013, 22 (**11**): 117901. DOI: 10.1088/1674-1056/22/11/117901

SPECIAL TOPIC — Laser and plasma assisted synthesis of advanced nanoparticles in liquids

Laser fragmentation in liquid synthesis of novel palladium-sulfur compound nanoparticles as efficient electrocatalysts for hydrogen evolution reaction

Guo-Shuai Fu(付国帅)[†], Hong-Zhi Gao(高宏志)[†], Guo-Wei Yang(杨国伟), Peng Yu(于鹏)[‡], and Pu Liu(刘璞)[§]

State Key Laboratory of Optoelectronic Materials and Technologies, Nanotechnology Research Center, School of Materials Science & Engineering, Sun Yat-sen University, Guangzhou 510275, *China*

(Received 13 November 2021; revised manuscript received 8 January 2022; accepted manuscript online 24 January 2022)

One promising way to tune the physicochemical properties of materials and optimize their performance in various potential applications is to engineer material structures at the atomic level. As is well known, the performance of Pd-based catalysts has long been constrained by surface contamination and their single structure. Here, we employed an unadulterated top-down synthesis method, known as laser fragmentation in liquid (LFL), to modify pristine PdPS crystals and obtained a kind of metastable palladium-sulfur compound nanoparticles (LFL-PdS NPs) as a highly efficient electrocatalyst for hydrogen evolution reaction (HER). Laser fragmentation of the layered PdPS crystal led to a structural reorganization at the atomic level and resulted in the formation of uniform metastable LFL-PdS NPs. Noteworthy, the LFL-PdS NPs show excellent electrocatalytic HER performance and stability in acidic media, with an overpotential of −66 mV at 10 mA·cm^{-2}, the Tafel slope of 42 mV·dec^{-1}. The combined catalytic performances of our LFL-PdS NPs are comparable to the Pt/C catalyst for HER. This work provides a top-down synthesis strategy as a promising approach to design highly active metastable metal composite electrocatalysts for sustainable energy applications.

Keywords: Pd-based electrocatalyst, hydrogen evolution reaction, laser fragmentation in liquid, nanoparticles

PACS: 79.20.Eb, 81.16.Hc, 82.45.Jn, 61.46.Df **DOI:** 10.1088/1674-1056/ac4e0e

1. Introduction

Hydrogen energy is considered to be an appealing green energy source for replacing fossil fuels due to its ultra-high energy density and environmental friendliness. Catalytic water splitting to produce hydrogen, with the advantages of high energy conversion efficiency, simple operation, and zero carbon emission, has been widely recognized as one of the most promising methods to obtain hydrogen.[1] To apply electrochemical water splitting successfully in actual work, it is necessary to develop catalysts with high activity, superior stability, and at a low cost. Platinum-based materials have long been considered to be the most efficient catalysts for the desorption of hydrogen from water, as the strength of the Pt–H bond is associated with the fastest reaction rate for the HER.[2] However, the application of platinum-based catalysts in HER is limited due to the high cost and low reserves of platinum resources on the earth. At present, there have been many reports of non-precious-metal-based electrocatalysts in the academic field, such as metal-free carbon,[3] transition metals,[4] transition metal oxides,[5] transition metal carbides,[6,7] transition metal sulfides,[8–10] and metal alloys.[11,12] However, the catalytic activity and stability of these catalysts are poor and hardly comparable to that of Pt-based catalysts.

Palladium-based (Pd-based) catalysts, which have attracted much attention in recent years, with its Gibbs free energy for atomic hydrogen adsorption (ΔG_{H*}) being very close to that of platinum, have been considered as an alternative HER electrocatalytic material with great potential.[13] For example, Pd-MoS_2,[14] Pd-CN_x,[15] PdMnCo/NC,[16] and Pd_4Se[17] have been reported showing excellent electrochemical performance under acidic conditions. However, most of these works also point out that the high dependence on a single structure of the reported Pd-based catalysts severely restricts their further improvement of the HER performance. Nevertheless, there was a report demonstrating that a kind of amorphous Li-PPS NDs,[18] which was obtained by using a simple lithium intercalation method to modify layered crystalline $Pd_3P_2S_8$, has shown an excellent electrochemical property. Their current density of 10 mA·cm^{-2} only needs a low overpotential of −91 mV, and the Tafel slope is 29 mV·dec^{-1}, which is equivalent to Pt/C. The activation of this catalytic activity is attributed to changes in morphology and structure (loss of crystallinity, formation of vacancies, *etc.*) during the lithiation process. The above Pd-based catalysts exhibit superior HER performance under acidic conditions. However, due to the greater Pd–H binding energy, the HER activity of Pd is severely constrained.[19] Therefore, it is important to develop a Pd-based HER catalyst with high activity as well as

[†]These authors contributed equally to this work.
[‡]Corresponding author. E-mail: yupeng9@mail.sysu.edu.cn
[§]Corresponding author. E-mail: liupu5@mail.sysu.edu.cn

© 2022 Chinese Physical Society and IOP Publishing Ltd

long-term stability. Most notably, the HER activity of palladium has been reported to have a significant particle size effect. When the particle size range of palladium nanoparticles is 3 nm–42 nm, the best HER catalytic activity is obtained at 20 nm.[20] Herein, we used the laser fragmentation in liquid method (LFL) to modify layered PdPS crystals to obtain a kind of metastable palladium sulfur compound nanoparticles (LFL-PdS NPs) with a uniform particle size of about 20 nm. With a small overpotential of −66 mV at a current density of 10 mA·cm^{-2}, a small Tafel slope of 42 mV·dec^{-1}, the LFL-PdS NPs have exhibited excellent HER activity and stability, outcompeting PdPS crystal (−470 mV and 149 mV·dec^{-1}, respectively), and even superior to the performance of the commercial Pt/C catalyst in 0.5-M H_2SO_4. The activation of the electrocatalytic activity of LFL-PdS NPs was considered to result from the transformation of morphology and structure of layered PdPS crystals during the laser-induced solid–liquid interaction process while avoiding the introduction of any impurities. Therefore, this work provided a simple and efficient method to build high-performance nanoparticle electrocatalysts by the way of morphology and structure changes induced by laser fragmentation in liquid.

2. Experimental

2.1. Preparation of LFL-PdS NPs

Preparation of PdPS nanoparticles is performed by laser fragmentation in liquid (LFL). The block layered PdPS crystal was ground, and 10 mg of the ground PdPS powder was dispersed in 50-ml isopropanol/water (volume ratio of isopropanol:water = 3:1) solution with a glass container. After ultrasonic dispersion, the glass container is fixed to a magnetic stirrer and the stirrer is allowed to stir continuously to get a uniform fragmentation while the Nd-YAG laser is used to converge. During the fragmentation process, the Nd-YAG laser was operated at its third harmonic (355-nm wavelength) and kept pulsed laser energy of 120 mJ with a pulse duration of 10 ns and frequency of 10 Hz for the 2-h pulsed laser action of the synthesis process. The obtained solution after laser fragmentation was dried in an oven at 60 °C to remove the moisture and obtain the LFL-PdS NPs nanocomposite in powdered form.

2.2. Materials characterization

G500 high-resolution thermal field emission scanning electron microscope (Gemini500), transmission electron microscope with an accelerating voltage of 200 kV (JEM-2010HR) and 300 kV (FEI Tecnai G2 F30) were used to characterize the structure and surface morphology of the sample. The phase analysis of the sample was carried out with the Rigaku RIGAKU powder x-ray diffractometer, and the x-ray diffraction pattern was obtained at a scanning speed of 2° per minute from 5° to 90°. The x-ray photoelectron spectroscopy (XPS) performs component analysis on the surface of the sample.

2.3. Electrochemical measurements

The HER measurements were tested on the Autolab workstation using a typical three-electrode system with a graphite rod as the counter electrode, Ag/AgCl as the reference electrode, and a catalyst-loaded glass carbon electrode (GCE) as the working electrode. The catalyst ink was prepared by dispersing 5 mg of LFL-PdS NPs in 1 ml of deionized water. After sonicated, the electrocatalyst ink (5 μl) was loaded onto a glassy carbon electrode (3 mm in diameter) as the working electrode and the catalyst-loaded GCE was dried at room temperature, then 5 μl of 5-wt% Nafion solution was added dropwise on the surface of the working electrode and dried at room temperature to protect the catalyst. Using the same method, the pristine PdPS crystal and 20% commercial Pt/C catalyst were used to modify the GCEs. The linear sweep voltammetry (LSV) was carried out in 0.5-M H_2SO_4 aqueous solution with a scan rate of 5 mV·s^{-1}. The set current density of the chronoamperometry durability test is 20 mA·cm^{-2}. The stability test of cyclic voltammetry is a continuous potential cycling in the potential window of −0.1 V to 0.25 V (*versus* RHE) at a scan rate of 100 mV·s^{-1}. After the potential cycle, the LSV curve was recorded at a scan rate of 5 mV·s^{-1}. Record the *CV* curve in the non-Faraday region (0.15 V to 0.45 V, versus to RHE) at different scanning rates to evaluate the ECSA. The scanning rate were 20, 40, 80, 120, 160, 200, and 240 mV·s^{-1} for LFL-PdS NPs, and 80, 120, 160, 200, 240, 280, and 320 mV·s^{-1} for PdPS crystal. Electrochemical impedance spectroscopy measurements were conducted with a frequency from 0.01 Hz to 10^5 Hz and amplitude of 10 mV at an overpotential of 66 mV (*versus* RHE).

3. Results and discussion

3.1. Characterization

The crystal structures of pristine PdPS crystals and LFL-PdS NPs were analyzed by XRD as shown in Fig. 1. The diffraction pattern for PdPS crystals shows eight obvious peaks at 13.34°, 23.1°, 25.46°, 25.88°, 26.78°, 29.98°, 31.52°,34.98°, 40.64°, 41.78°, corresponding to (200), (111), (310), (211), (400), (311), (020), (411), (511), (321) crystal planes in the standard spectrum of PdPS (ICSD 2331), respectively. The positions of the diffraction peaks are unchanged, and the XRD patterns of the powders are consistent with the standard spectra of the PdPS crystals, indicating that the original PdPS material used for laser fragmentation in liquid (LFL) is a highly crystalline pure-phase PdPS crystal. When LFL was performed to treat samples, the high local pressure and high temperatures of several thousand degrees celsius increase the internal defects of the material, deteriorate the crystallinity,

and cause the appearance of metastable phases. The structural defects inside the sample are beneficial to improve the electrocatalytic properties of the material.[21] The LFL-PdS NPs sample shows a sharp diffraction peak at 13.3°, 25.46°, 26.8°, corresponding to the (200), (310), (400) crystal planes of the PdPS crystal.[22] The diffraction peak of LFL-PdS NPs appearing at 39° corresponds to the (111) crystal plane of Pd, indicating the precipitation of Pd. At the same time, the diffraction peak intensity decreases, and the half-height width increases, indicating the fragmentation and size reduction of PdPS crystals and the appearance of nanocrystals during the laser fragmentation in liquid. LFL is a promising method for the preparation of amorphous nanoparticles.[23]

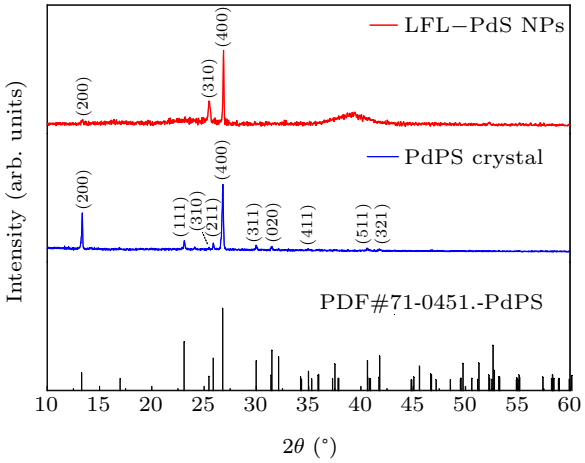


Fig. 1. XRD crystal structure analysis of PdPS crystal and LFL-PdS NPs.

To observe the morphological changes brought about by the laser for the pristine material, the samples were characterized using a G500 high-resolution thermal field emission scanning electron microscope. The SEM images of PdPS crystals, shown in Fig. 2(a), reflect the irregular lamellar structure of the PdPS crystal. The SEM images of LFL-PdS NPs are shown in Figs. 2(b)–2(c). The layered PdPS crystals are fragmented by laser action and subsequently formed into nanoparticles with a diameter of about 20 nm by the cooling effect of the surrounding liquid and its surface tension. The nanospheres are tightly arranged and uniformly distributed, exposing a large number of active sites, which is conducive to improving the electrochemical properties of the material. It has been studied that surface Pd nanoparticles have a significant particle size effect, and a particle size of 20 nm has the best HER activity.

The morphology and structure of PdPS crystals before and after the LFL process were further characterized by TEM. The PdPS crystals were formed by stacking thin sheets together, and the stacked sheets can be seen, with clear lattice stripes and diffraction spots, indicating the good crystallinity of the original PdPS crystals (Figs. 2(d)–2(e)). Figure 2(f) shows a typical low-magnification transmission electron microscopy (TEM) image of the LFL-PdS NPs, in which a batch of spherical nanoparticles is developed from the fragmentation of flaky PdPS crystals under the action of the laser. Polycrystalline rings can be seen after LFL-PdS NPs undergo selected area diffraction (Fig. 2(f)). High-resolution transmission electron microscopy (HRTEM) was used to characterize the LFL-PdS NPs (Fig. 2(g)). The lattice fringes of LFL-PdS NPs display interplanar spacings of 0.23 nm in the particle, corresponding to the (111) crystal plane of Pd, which match well with the crystallographic spacing of the broad peak corresponding to 2θ of 39° in XRD powder diffraction. Some of the lattice stripes outside the white box are disordered and indistinct, indicating that the local extreme environment in the LFL led to the formation of amorphous regions. LFL-PdS NPs are a mixed state consisting of amorphous and nanocrystalline structures. In addition, to determine the elemental content, distribution and structural characteristics of LFL-PdPS NPs, an EDS line scan of the sample was performed. EDS elemental analysis of the green area in Fig. 2(h) showed that the percentage of Pd atoms was 71.37%, the percentage of P atoms was 15%, and the percentage of S atoms was 13.63%, with a ratio of roughly 5:1:1 (Fig. 2(i)). Figure 2(j) shows the distribution of Pd, P, and S elements. As seen that Pd elements are mainly concentrated on the nanospheres, P elements are mainly distributed in the area outside the nanospheres, and S elements are more uniformly distributed. The Pd–P bond in the PdPS crystal is so weak that it is easily broken under the action of a longtime highenergy laser. P almost does not exist inside the PdS nanoparticles but exists in the form of phosphate. The Pd and S elements form nanospheres as PdS compounds, while the Pd–S bond is also partially broken and the S element exists in the form of sulfate. This result can correspond to the XPS results (Fig. 3).

The surface analysis of LFL-PdS NPs was carried out using x-ray photoelectron spectroscopy (Fig. 3). From Fig. 3(a), it is clear that LFL-PdS NPs contain three elements, S, P, and Pd, indicating that all of the elements are preserved after the LFL of the PdPS crystal. Figures 3(b)–3(d) show the XPS spectra of Pd 3d, P 2p, and S 2p. The Pd $3d_{5/2}$ and $3d_{3/2}$ peaks are observed at 336.1-eV and 341.5-eV components of Pd, suggesting the formation of Pd clusters, respectively. Two additional small peaks at 336.61 eV and 341.87 eV are also observed in the spectrum, which might be attributed to the small amount of Pd^{2+} from residual PdPS crystals[24] (Fig. 3(b)). LFL-PdS NPs retained only the peaks at 134.23 eV corresponding to phosphate[25,26] (Fig. 3(c)). The phosphate may come from the phosphate adsorbed on the surface of LFL-PdS NPs, which indicates that the P may be detached from the material during the reaction, thus forming a large number of P vacancies that can enhance HER activity.[27] And then, double peaks of S 2p appeared at 162.79 eV and 163 eV, corresponding to $2p_{3/2}$ and $2p_{1/2}$,[28] as shown in Fig. 3(d). In addition, the peak of sulfate appears at 167.59 eV. Furthermore, the C 1s spectrum was fitted for three peaks of 284.58, 285.78, and 288.33 eV which match the standard signals of amorphous carbon shell.[29–32]

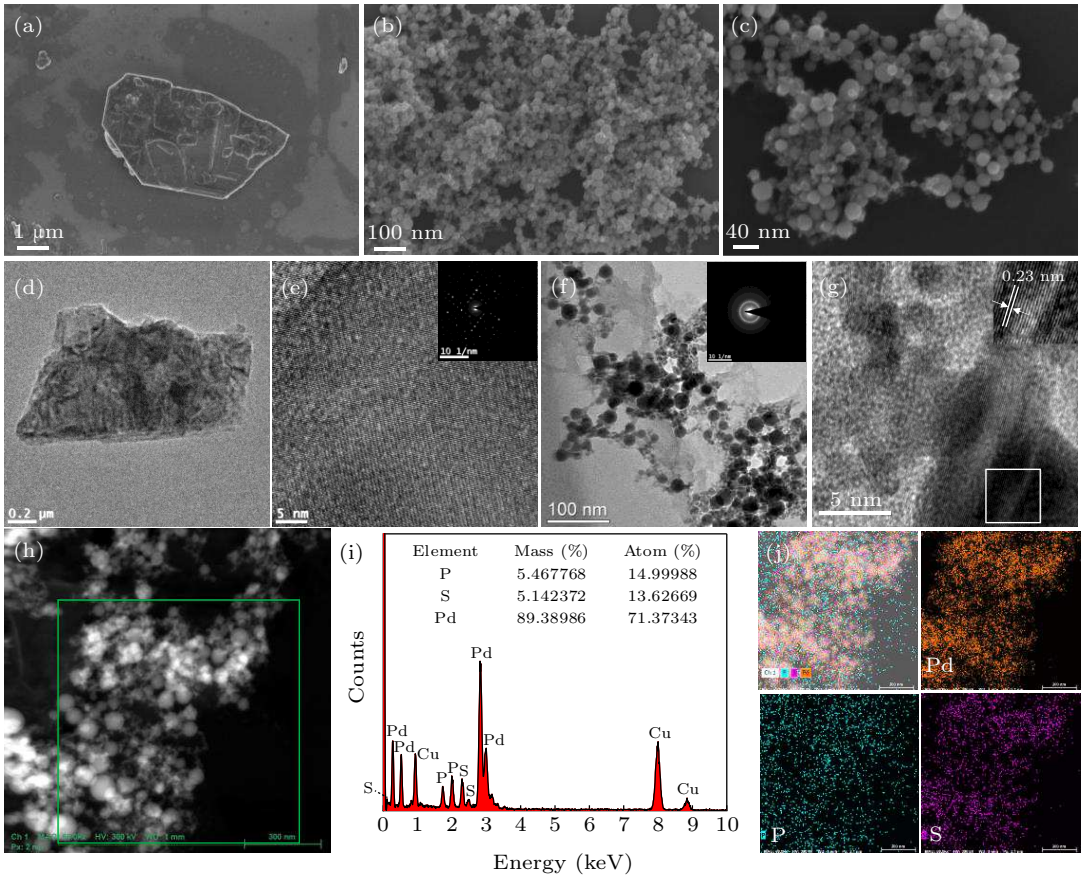


Fig. 2. (a) SEM images of the PdPS crystal, (b)–(c) SEM images of LFL-PdS NPs, (d) TEM images of PdPS crystals, (e) HRTEM images and corresponding electron diffraction patterns of PdPS crystals, (f) TEM images of LFL-PdS NPs and corresponding electron diffraction patterns, (g) HRTEM images of LFL-PdS NPs, (i) EDS spectra of LFL-PdS NPs, (j) the elemental distribution of LFL-PdS NPs.

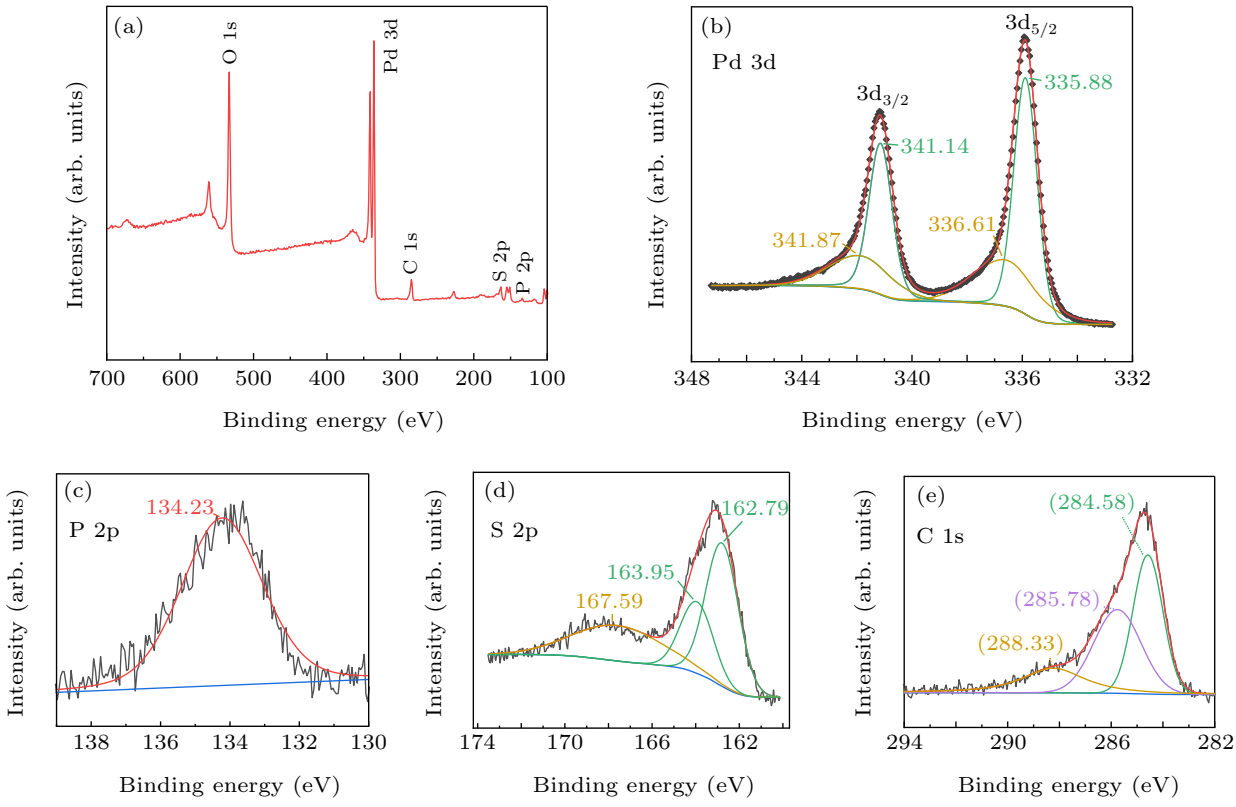


Fig. 3. XPS spectra of LFL-PdS NPs: (a) full XPS spectra, (b) P 2p spectra of XPS, (c) S 2p spectra of XPS, (d) Pd 3d spectra of XPS, (e) C 1s spectra of XPS.

3.2. Electrochemical activity

The HER performance of LFL-PdS NPs was investigated in a 0.5-M H_2SO_4 aqueous solution and compared with commercial Pt/C catalysts (20 wt%), PdPS crystals. Figure 4(a) displays the HER polarization curves obtained from linear sweep voltammetry (LSV) measurements. LFL-PdS NPs show a very small onset potential value of −8.5 mV *versus* RHE, much smaller than that of PdPS crystal (−144 mV) (Fig. 4(a)). Moreover, LFL-PdS NPs (Tafel slope: 42 mV·dec^{-1}) (Fig. 4(b)) exhibit higher catalytic activity compared to PdPS crystals (Tafel slope: 149 mV·dec^{-1}); its activity is close to that of commercial Pt/C (Tafel slope: 39 mV·dec^{-1}). Such a small Tafel slope indicates faster kinetics of the catalytic reaction of LFL-PdS NPs with the Volmer–Tafel mechanism acting as the HER pathway.[33] The binding of adsorbed hydrogen atoms in this process becomes the rate-limiting step of the hydrogen evolution reaction.[34] The faster catalytic reaction kinetics allows the laser-treated LFL-PdS NPs to reach high current densities with a low overpotential: 10 mA·cm^{-2} at −66 mV and 50 mA·cm^{-2} at −133 mV. As shown in Fig. 4(a), its operating potential is already very close to that of the commercial Pt/C catalyst −55 mV.

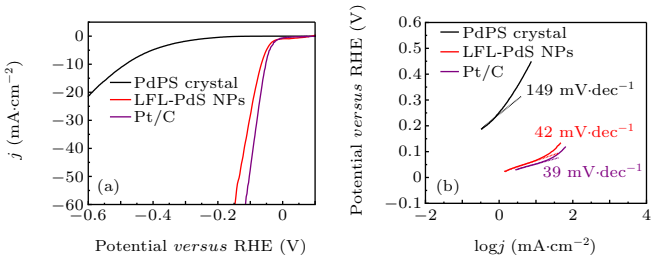


Fig. 4. (a) Polarization curves of PdPS crystal, LFL-PdS NPs, 20% commercial Pt/C catalyst in 0.5-M H_2SO_4, (b) the corresponding Tafel slope.

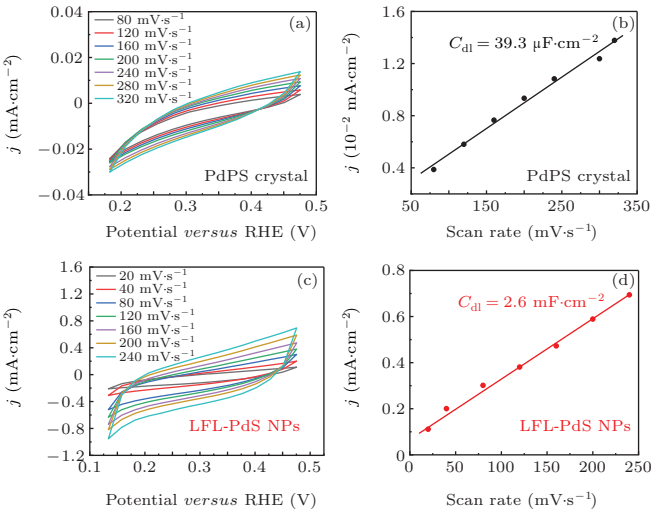


Fig. 5. (a) and (c) Measurement of double-layer capacitance (C_{dl}) in 0.5-M H_2SO_4 by cyclic voltammetry, (b) double-layer capacitance diagrams of LFL-PdPS, (d) double-layer capacitance diagrams of PdPS crystal.

To evaluate the activity of LFL-PdS NPs, the electrochemically active surface areas (ECSA) of LFL-PdS NPs and PdPS crystals were compared by calculating the electrochemical bilayer capacitance (C_{dl}). The ECSA represents the intrinsic electrocatalytic activity of the electrocatalyst and is related to the number of active sites as well as the electrical conductivity of the catalyst.[35] As shown in Fig. 5(a)–5(d), the C_{dl} of LFL-PdS NPs is 2.6 mF·cm^{-2} (Fig. 5(d)), which is much higher than the C_{dl} of PdPS crystals (C_{dl} = 39.3 μF·cm^{-2}) (Fig. 5(b)). The higher C_{dl} of LFL-PdS NPs indicates that laser fragmentation in liquid leads to a larger electrochemical active area of LFL-PdS NPs, and the intrinsic activity and number of active sites are better than those of PdPS crystals. Electrochemical impedance spectroscopy was carried out on LFL-PdS NPs and PdPS crystals. As can be seen from Fig. 6, the charge transfer impedance R_{ct} of LFL-PdS NPs is significantly smaller than that of the PdPS crystal, indicating that LFL-PdS NPs possess a faster electrocatalytic kinetic behavior.

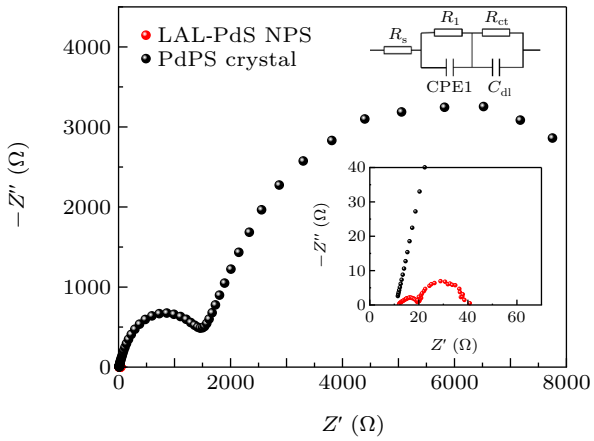


Fig. 6. EIS Nyquist plots for the LFL-PdS NPs and PdPS crystal and the corresponding Randies equivalent circuit diagram.

In addition, LFL-PdS NPs have remarkable durability in HER. As shown in Fig. 7(a), the polarization curve obtained is only slightly negatively shifted, and the overpotential at 10 mA·cm^{-2} is only negatively shifted by 5 mV after 10^4 cyclic voltammetry cycles. Moreover, the chronopotentiometry measurements indicate that LFL-PdS NPs possess excellent long-term operation stability at 20 mA·cm^{-2} (Fig. 7(b)).

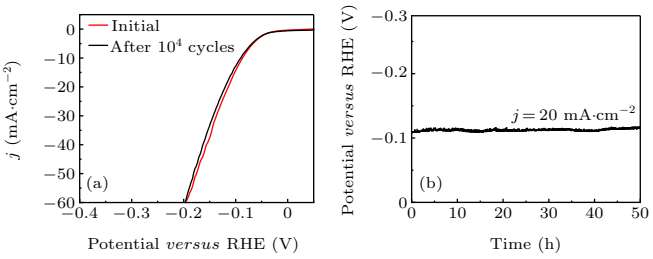


Fig. 7. Stability test of LFL-PdS NPs in the HER. (a) Polarization curves of LFL-PdS NPs before and after 10^4 cyclic voltammetry tests between −0.15 V and 0.25 V (*versus* RHE). (b) Chronoamperometric measurements of LFL-PdS NPs under j = 20 mA·cm^{-2} in 0.5-M H_2SO_4 aqueous solution.

3.3. HER enhancement mechanism

Based on the excellent HER activity of LFL-PdS NPs prompted us to probe the enhanced mechanism. Recently,

Yang and co-workers have found that amorphization of palladium sulfides could be possible to enhance the activity towards the HER.[36] This may be the reason why our LFL-PdS NPs exhibit excellent activity. Furthermore, the conductivity of the catalyst is improved due to the precipitation of Pd clusters. The electrochemical impedance spectroscopic data (Fig. 6) show a charge transfer resistance, R_{ct} of 10 Ω for the LFL-PdS NPs while the value obtained is 1700 Ω for bulk PdPS. Mechanistically, the hydrogen evolution reaction is generally Volmer–Heyrovsky or Volmer–Tafel mechanism.[37] Three possible principal steps are involved in the electrochemical HER process as given below:[38]

Volmer reaction (electrochemical hydrogen adsorption)

$$H_3O^+ + M + e^- \rightarrow M - H^* + H_2O. \quad (1)$$

Heyrovsky reaction (electrochemical desorption)

$$M - H^* + e^- + H^+ \rightarrow H_2 + M. \quad (2)$$

Tafel reaction (chemical desorption)

$$2M - H^* \rightarrow H_2 + 2M. \quad (3)$$

Generally, the hydrogen adsorption energy is considered as a criterion for the performance of HER catalysts. There are two processes of hydrogen adsorption and desorption steps on the catalyst surface, a suitable hydrogen adsorption energy is required to facilitate the hydrogen adsorption and desorption at the same time. The Tafel slope of 42 mV·dec^{-1} suggests that a Heyrovsky-reaction-determined Volmer–Heyrovsky mechanism works in the LFL-PdS NPs catalyst (Fig. 4(b)). The bulk PdPS however, shows a Tafel slope of 149 mV·dec^{-1} revealing that the Volmer reaction is slow. Hence, we speculate that during the laser fragmentation process, the escape of P atoms causes the PdS atoms to re-bond. This process may improve the hydrogen adsorption energy and make it easier to adsorb hydrogen.

4. Conclusion

In summary, by introducing processes of LFL-induced structural engineering, we developed a top–down method to prepare LFL-PdS nanoparticles by modifying PdPS crystals through laser fragmentation in liquid. The prepared novel metastable LFL-PdS composite nanoparticles (LFL-PdS NPs) presented regular spherical nanometrology with smooth surface and uniform particle size distributions, meanwhile possessing excellent HER activity and stability. In acidic media, LFL-PdS NPs have excellent HER activity, very close to that of commercial Pt/C. The overpotential for LFL-PdS NPs at 10 mA·cm^{-2} is only −66 mV and the Tafel slope is 42 mV·dec^{-1}. More attractively, the LFL-PdS NPs exhibit excellent stability in the HER process, which simultaneously solves the catalytic activity and stability problems of Pd-based catalysts. Our structural engineering strategy of this work provided an avenue to tune and prepare crystal structures of two-dimensional materials with unique properties and enhanced performances, which could be used for various research on further promising functional nanomaterial applications.

Acknowledgments

Project supported by the Natural Science Foundation of Guangdong Province, China (Grant No. 2016A030313339), the Science and Technology Planning Project of Guangdong Province, China (Grant No. 2017B090918002), the National Key Basic Research Program of China (Grant Nos. 2014CB931700 and 2017YFA020623), the National Natural Science Foundation of China (Grant Nos. 51832011 and 91833302), and the Fund from State Key Laboratory of Optoelectronic Materials and Technologies (Grant No. OEMT-2021-PZ-02).

References

[1] Khan M A, Zhao H, Zou W, Chen Z, Cao W, Fang J, Xu J, Zhang L and Zhang J 2018 *Electrochem. Energy Rev.* **1** 483
[2] Popczun E J, Read C G, Roske C W, Lewis N S and Schaak R E 2014 *Angew. Chem. Int. Ed.* **53** 5427
[3] Ito Y, Cong W, Fujita T, Tang Z and Chen M 2015 *Angew. Chem. Int. Ed.* **54** 2131
[4] Ahn S H, Hwang S J, Yoo S J, Choi I, Kim H J, Jang J H, Nam S W, Lim T H, Lim T, Kim S K and Kim J J 2012 *J. Mater. Chem.* **22** 15153
[5] Tang Y J, Gao M R, Liu C H, Li S L, Jiang H L, Lan Y Q, Han M and Yu S H 2015 *Angew. Chem. Int. Ed.* **54** 12928
[6] Fan X, Peng Z, Ye R, Zhou H and Guo X 2015 *ACS Nano* **9** 7407
[7] Esposito D V, Hunt S T, Kimmel Y C and Chen J G 2012 *J. Am. Chem. Soc.* **134** 3025
[8] Morales-Guio C G and Hu X 2014 *Acc. Chem. Res.* **47** 2671
[9] Niu Y, Li W, Wu X, Feng B, Yu Y, Hu W and Li C M 2019 *J. Mater. Chem. A* **7** 10534
[10] Yang L, Xiao X, Yang Z, Cai Y, Xie B, Zhao N, Li X, Wang Y, Liu M, Wang X, Wang G, Gan Z, Meng M, Yang W, Zhang J and Liu J M 2018 *Int. J. Hydrogen Energy* **43** 15135
[11] Cardoso D S P, Eugénio S, Silva T M, Santos D M F, Sequeira C A C and Montemor M F 2015 *RSC Adv.* **5** 43456
[12] Adit M T and Peterson A A 2014 *J. Phys. Chem. C* **118** 4275
[13] Sarkar S and Peter S C 2018 *Inorg. Chem. Front.* **5** 2060
[14] Luo Z, Ouyang Y, Zhang H, Xiao M, Ge J, Jiang Z, Wang J, Tang D, Cao X, Liu C and Xing W 2018 *Nat. Commun.* **9** 2120
[15] Bhowmik T, Kundu M K and Barman S 2016 *ACS Catal.* **6** 1929
[16] Zhang R, Sun Z, Feng R, Lin Z, Liu H, Li M, Yang Y, Shi R, Zhang W and Chen Q 2017 *ACS Appl. Mater. Interfaces* **9** 38419
[17] Kukunuri S, Austeria P M and Sampath S 2016 *Chem. Commun. (Camb)* **52** 206
[18] Zhang X, Luo Z, Yu P, Cai Y, Du Y, Wu D, Gao S, Tan C, Li Z, Ren M, Osipowicz T, Chen S, Jiang Z, Li J, Huang Y, Yang J, Chen Y, Ang C Y, Zhao Y, Wang P, Song L, Wu X, Liu Z, Borgna A and Zhang H 2018 *Nat. Catal.* **1** 460
[19] Zhu J, Hu L, Zhao P, Lee L Y S and Wong K Y 2020 *Chem. Rev.* **120** 851
[20] Zheng J, Zhou S, Gu S, Xu B and Yan Y 2016 *J. Electrochem. Soc.* **163** F499
[21] Tiwari J N, Harzandi A M, Ha M, Sultan S, Myung C W, Park H J, Kim D Y, Thangavel P, Singh A N, Sharma P, Chandrasekaran S S, Salehnia F, Jang J W, Shin H S, Lee Z and Kim K S 2019 *Adv. Energy Mater.* **9** 1900931
[22] Jeitschko W 1974 *Acta Cryst. B* **30** 2565
[23] Zhu J, Hu S, Wang W, Xia W W, Chen H T and Chen X B 2017 *Appl. Phys. A* **123** 244
[24] Liang S X, Zhang L C, Reichenberger S and Barcikowski S 2021 *Phys. Chem. Chem. Phys.* **23** 11121

[25] Kibis L S, Titkov A I, Stadnichenko A I, Koscheev S V and Boronin A I 2009 *Appl. Surf. Sci.* **255** 9248
[26] Grasso V and Silipigni L 2003 *J. Vac. Sci. Technol. A* **21** 860
[27] Duan J, Chen S, Ortiz-Ledon C A, Jaroniec M and Qiao S Z 2020 *Angew. Chem. Int. Ed.* **59** 8181
[28] Zubavichus Y V, Golub A S, Novikov Y N, Slovokhotov Y L, Nesmeyanov A N, Schilling P J and Tittsworth R C 1997 *J. Phys. IV* **7** 1057
[29] Amendola V, Amans D, Ishikawa Y, Koshizaki D, Sciré S, Compagnini G, Reichenberger S and Barcikowski S 2020 *Chem. Eur. J.* **26** 9206
[30] Zhang D S, Zhang C, Liu J, Chen Qi, Zhu X G and Liang C H 2019 *ACS Appl. Nano Mater.* **2** 28
[31] Gaashani R A, Najjar A, Zakaria Y, Mansour S and Atieh M A 2019 *Ceram. Int.* **45** 14439
[32] Wang X F, Feng Z J, Huang J T, Deng W, Li X B, Zhang H S and Wen Z H 2018 *Carbon* **127** 149
[33] Zhang L, Si R, Liu H, Chen N, Wang Q, Adair K, Wang Z, Chen J, Song Z, Li J, Banis M N, Li R, Sham T K, Gu M, Liu L M, Botton G A and Sun X 2019 *Nat. Commun.* **10** 4936
[34] Shinagawa T, Garcia-Esparza A T and Takanabe K 2015 *Sci. Rep.* **5** 13801
[35] Liu D, Li X, Chen S, Yan H, Wang C, Wu C, Haleem Y A, Duan S, Lu J, Ge B, Ajayan P M, Luo Y, Jiang J and Song L 2019 *Nat. Energy* **4** 512
[36] Wang Y H, Xu K, Zhu Z Z, Guo W, Yu T T, He M S, Wei W X and Yang T 2021 *Chem. Commun.* **57** 1368
[37] Eftekhari A 2017 *Int. J. Hydrog.* **42** 11053
[38] Conway B E and Tilak B V 2002 *Electrochim. Acta* **47** 3571